Adsorption (2006) 12:405–416
DOI 10.1007/s10450-006-0568-7

Interpretation of chromatographic retentions of simple solutes with an amylose-based sorbent using infrared spectroscopy and DFT modeling

Rahul B. Kasat · Chim Y. Chin · Kendall T. Thomson · Elias I. Franses · Nien-Hwa Linda Wang

Abstract The interactions of amylose tris(3,5-dimethylphenylcarbamate) (ADMPC, commercially "Chiralpak AD") with 10 simple solutes—1-propanol, heptane, heptanol, benzene, propylbenzene, benzyl alcohol, pyridine, tetrahydrofuran, diethylamine, and aniline—are studied using attenuated total reflection infrared spectroscopy (ATR-IR) of thin polymer films, DFT modeling, and high performance liquid chromatography (HPLC). ATR-IR is used to determine the changes in the hydrogen bonding states of the C═O and NH groups of the polymer amide I and II bands upon absorption of each of the solutes at 25°C. DFT modeling with B3LYP/6-311+g(d,p) level of theory is used to predict the IR wavenumbers, the H-bonding interaction energies, and the hydrogen bonding distances of the polymer side-chains with certain solute molecules. The capacity factors of these solutes with ADMPC have been measured at 25°C in hexane/isopropanol (95/5, v/v) solvent. From IR data and DFT modeling, we conclude that the C═O and NH are key binding sites of the polymer and interact with the functional groups of various solutes. The capacity factors are understood on the basis of hydrogen bonding, hydrophobic, and dipole-dipole interactions of the C═O, NH, and phenyl groups of the sorbent with OH, NH, NH_2, O, phenyl, and N functional groups of the solutes.

Keywords Capacity factors · Chiral separation · Amylose tris(3,5-dimethylphenylcarbamate) · Hydrogen bonding · Hydrophobic interactions · Dipole-dipole interactions

R. B. Kasat · C. Y. Chin · K. T. Thomson · E. I. Franses (✉) · N.-H. Linda Wang (✉)
School of Chemical Engineering, Purdue University, 480 Stadium Mall Drive, West Lafayette, IN 47907-2100
e-mail: wangn@ecn.purdue.edu

E. I. Franses
e-mail: franses@ecn.purdue.edu

C. Y. Chin
Present address:
PureVision Technology Inc., 511 N. McKinley, Ft. Lupton, CO 80621

1 Introduction

Chiral molecules, such as amino acids, carbohydrates, and nucleic acids, play important roles in physiological processes. Different stereoisomers of chiral pharmaceutical drugs can interact differently with biological chiral sites, such as receptors, enzymes, and ion channels (Agranat et al., 2002). If one enantiomer is therapeutically active, the other could be inactive, or an antagonist, or have a different or undesirable activity (Agranat et al., 2002). According to the FDA, the enantiomers of a drug should be separated and tested for their pharmacodynamic and pharmacokinetic effects before they can be approved for patient use. If each enantiomer cannot be synthesized separately at a low cost, one may synthesize the racemic mixture and separate the enantiomers.

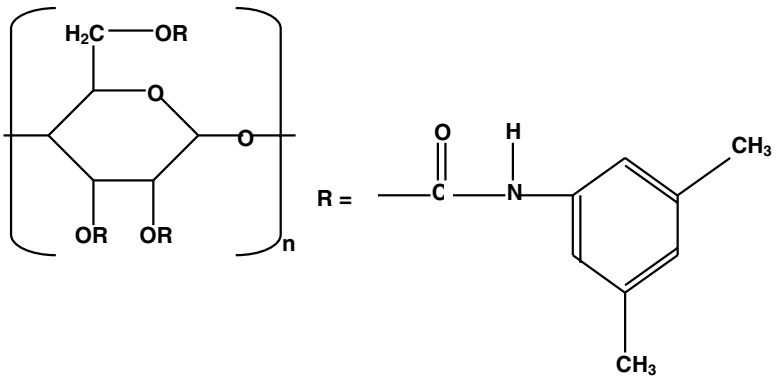

Fig. 1 Molecular structure of derivatised amylose used, amylose tris(3,5-dimethylphenylcarbamate) (ADMPC); R is the side-chain

High performance liquid chromatography (HPLC) is widely used commercially for analytical or preparative separation of chiral enantiomer drugs. Many types of chiral stationary phases (sorbents) have been developed with a significant selectivity, or "molecular recognition", of chiral enantiomers (Pirkle et al., 1980; Armstrong and Demond, 1984; Okamoto et al., 1987a; Jadaud and Wainer, 1989; Armstrong et al., 1994; Lammerhofer and Lindner, 1996). A major class of sorbents has polymer films of derivatized polysaccharides (Yashima, 2001) deposited in the pore surfaces of porous silica beads. Okamoto et al. synthesized such sorbents starting from available biopolymers, such as cellulose and amylose (Okamoto et al., 1987a,b). An important example is amylose tris(3,5-dimethylphenylcarbamate) (ADMPC, Fig. 1). The commercial product "Chiralpak AD", with which a wide variety of chiral molecules can be separated, contains primarily ADMPC polymer deposited in porous silica beads (Okamoto and Yashima, 1998; Yashima, 2001; Yashima and Okamoto, 2004). The recognition mechanism of this sorbent remains to be elucidated completely (Yamamoto et al., 2002).

Several studies have focused on the possible structure and the possible chiral discrimination mechanisms of ADMPC. A structural analysis of low molecular weight ADMPC using 2D solution-state NMR suggests that the polymer forms rods which are helical. Molecular mechanics simulations were done to elucidate the solute-sorbent binding and the chiral discrimination mechanism (Yamamoto et al., 2002). Solid state NMR was used to study the structural effects of the polymer sorbent as a function of the mobile phase ("solvent") composition (Wenslow and Wang, 2001). The changes observed in the NMR spectra of the sorbent upon the contact with the solvent were attributed to crystallinity changes of the polymer. The retention times data of a series of chiral arylcarboxylic acid solutes were correlated with a series of molecular descriptors, to produce quantitative structure-enantioselective retention relationships (QSERR) incorporating the hydrogen bonding ability and aromaticity of the solutes (Booth and Wainer, 1996).

Most of the chiral molecules used for various applications (pharmaceuticals, fungicides, etc.) are quite complex with many functional groups, several of which (3 or more) may need to interact with the functional groups or potential binding sites of the sorbent for proper enantiomer discrimination (Chilmonczyk et al., 1999; Caccamese and Principato, 2000; Wang et al., 2000; Goossens et al., 2005). The relative contribution of each functional group on the capacity factors should be studied in detail in order to understand the discrimination mechanism of complex chiral molecules. In this article, to elucidate the effect of the relative strength of different functional groups on the capacity factor, ten simple non-chiral solutes—alcohols, alkanes, aromatics, and other solutes—having typical (common) functional groups are chosen, and their interactions with ADMPC polymer are probed using chromatography, and infrared spectroscopy. The solute functional groups are mainly OH, Phenyl, NH, NH_2, CH, N, and O. The types of solute-sorbent interactions which may be important for this class of sorbents are hydrogen bond (H-bond), hydrophobic interactions (primarily aromatic-aromatic or π-π, dispersive), other dipole-dipole, and dipole-induced dipole interactions. The C=O and NH groups from the side-chains and the oxygen atoms from the backbone of the ADMPC sorbent (Fig. 1) can interact with the

solutes and the solvents via H-bond interactions. The C═O groups can also interact with the solutes and the solvents via dipole-dipole interactions also. The aromatic rings and CH_3 groups of the sorbent can interact mainly with phenyl or aliphatic groups via hydrophobic interactions.

The primary goal of this article is to identify the binding sites of the ADMPC polymer and understand the molecular level interactions of these sites with simple solutes with one or two functional groups using attenuated total reflection infrared spectroscopy (ATR-IR) and DFT modeling. The second goal is to study how the capacity factors of these solutes measured in chromatography are linked to solute-sorbent, solute-solvent, and solvent-sorbent interactions. Such understanding is an important step for selecting the optimum sorbent and solvent for chromatographic separations. Some potential interactions between the sorbent and the solute functional groups are summarized in Table 1.

This article is organized as follows. First, certain H-bonding interactions between the ADMPC and each of the solutes are probed with ATR-IR spectroscopy. Then, certain such interactions between the polymer side-chains and some solutes functional groups are modeled and quantified using DFT calculations to obtain more detailed insights. Finally, the measured solutes capacity factors, as determined from HPLC data, are related to certain molecular interactions established with IR. We conclude that the C═O and NH groups of the polymer are the main binding sites and interact with the functional groups of different solutes via H-bond and dipole-dipole interactions. Furthermore, the chromatographic retentions of the different solutes with the polymer are explained in detail using IR and DFT modeling.

2 Materials and methods

2.1 Materials

Aniline, heptane, tetrahydrofuran (THF), dimethylacetamide (DMAc), dimethylformamide (DMF), and chloroform were purchased from Mallinckrodt Chemicals (Phillipsburg, NJ); 1-heptanol, pyridine, diethylamine (DEA), propylbenzene, and 1,3,5-tri-tert-butylbenzene (TTBB) were purchased from Sigma-Aldrich (Milwaukee, WI); 1-propanol, and benzene were purchased from J. T. Baker Co. (Phillipsburg, NJ); benzyl alcohol was purchased from Fisher Chemicals (Fair Lawn, NJ). Semipreparative ChiralPak AD columns (100 mm long $\times$10 mm diameter) with 20 μm diameter particles were provided by Chiral Technologies Inc. (Exton, PA). The estimated interparticle void fraction ε_b was 0.32, and the estimated intraparticle void fraction ε_p was 0.55 (Lee et al., 2005).

2.2 In-situ ATR-FTIR spectroscopy

A Nicolet Protégé 460 Fourier transform infrared spectrometer, equipped with an MCT detector cooled with liquid nitrogen, was used to obtain all FTIR spectra. Spectral contributions from water vapor and carbon dioxide were minimized by continuously purging the instrument's sample chamber with dry air from a Balston purge gas generator. ATR spectra were collected with unpolarized incident light at 25°C using a custom-made accessory. The incident angle was typically 50°, with the number of reflections being 7. All spectra were taken at a resolution of 2 cm^{-1} using Happ-Genzel apodization. The Si-ATR plates have absorption cut-off at about 1500 cm^{-1}. All spectra were collected using 256 scans.

Table 1 Potential solute-sorbent interactions for ADMPC (Fig. 1) with the solutes studied

Type	Sorbent···Solute
H-bond	C = O···HO (alcohols, water)
H-bond	NH···OH (alcohols, water)
H-bond	NH···NH (amines)
H-bond	HN···H_2N/HN (amines)
H-bond	NH···:N (pyridine)
H-bond	NH···:O (tetrahydrofuran)
H-bond	C═O···HC (pyridine, tetrahydrofuran)
Hydrophobic	Aromatic···Aromatic (aromatics)
Hydrophobic	Hydrocarbon···Hydrocarbon
Dipole-dipole	C═O···Benzene, Pyridine, THF, DEA, Aniline

ATR-IR spectra were obtained using the polymer films deposited on the Si-ATR plates instead of using silica beads containing polymer inside the pores for higher sensitivity. Transmission infrared spectroscopy (T-IR) can also be used for the dry silica beads, but was not used here because some of the solutes could dissolve the IR windows. Polymer films for these experiments were prepared as follows. The ADMPC polymer was dissolved in DMF at 60°C and then cooled to room temperature. The polymer was spin coated on Si-ATR plates (Wilmad, NJ) using a WS-400A-6NPP-Lite Spin Processor, at a spinning speed of 500 rpm for 5 min. The thicknesses of these films were about 1 to 10 μm. The films were annealed in a vacuum oven for at least 1 h at 80°C. There was no dependence of the IR spectrum of the dry polymer film on the solvent used for deposition (DMF, THF, or DMAc). In-situ spectra of the films on the Si-ATR plates in contact with a solute were obtained with a liquid cell from Harrick Scientific (Ossining, NY). Since the film thickness was ca. 1–10 μm, only a small fraction, if any, of the film may be affected by the interaction with the surface. For this reason, and since the exact surface chemistry of the commercial silica beads was not known to us, we used silicon oxide on silicon as a substrate surface.

2.3 Computational methodology

For simplicity in the density functional theory (DFT) calculations, a single side-chain was chosen to interact with a solute in two different conformations. The geometry optimization calculations for minimum energy were performed using Gaussian 03 program (Frisch et al., 2004). These calculations are relevant for small solutes. For large solutes, the whole polymer rod or solid structure may need to be modeled. This is beyond the scope of this article. The polymer side-chain was modeled first alone, in order to calculate the wavenumbers of the amide I and II bands. The side-chain was then allowed to form a complex with one solute molecule at a time. The IR wavenumbers of the amide groups, H-bond interaction energies, H-bond distances, and H-bond angles were calculated, to assess the strengths of the possible H-bonds. Two simulations were done for certain solutes studied here by IR and HPLC. In one simulation, the solute molecule, acting as an H-bond acceptor, was placed near the C=O group of the polymer (Fig. 1). In the second one, the solute molecule acting as an H-bond donor, was placed near the NH group of the polymer. The resulting complexes were then energy-minimized. These calculations account primarily for the local interactions of solute molecules with the polymer side-chains and allow testing certain H-bonds hypotheses generated from the IR data.

DFT/B3LYP/6-311+g(d, p) level of theory was used. The B3LYP hybrid functional (Becke, 1993), which includes a mixture of Hartree-Fock exchange with DFT exchange-correlation, gives good intermolecular geometries and intermolecular vibrational frequencies predictions, which are similar to those obtained using MP2 (Meyer et al., 2001) for the calculations. Basis sets at the 6-311+g(d, p) level (triple-ζ level) have polarization functions on non-hydrogen and hydrogen atoms, and diffused functions with diffuse sp-shell on non-hydrogen atoms (Scheiner, 1997). The calculated IR wavenumbers were scaled by 0.96 for significantly better accuracy by accounting for the effect of an artificial stabilization of the complex due to a larger basis set, in comparison to the smaller sets of the individual molecules (Scheiner, 1997; Andersson and Uvdal, 2005). The counterpoise corrected method was used to compute basis set superposition error (BSSE) (Simon et al., 1996).

2.4 Chromatography apparatus and procedures

The HPLC apparatus consisted of a Degassit 6324 degasser, a Waters 515 HPLC pump, a Rheodyne 7725i injection valve, a Waters 996 photodiode array (PDA) UV detector, a Waters 2414 refractive index (RI) detector, and a personal computer (PC) with Waters Millennium software. Chromatographic fittings, PEEK tubing, and PEEK injection loops were purchased from Upchurch Scientific (Oak Harbor, WA). The mobile phase Hexane/IPA (95/5, v/v) was degassed for at least 30 min prior to use with a Branson 8510 sonicator. All chromatography experiments were carried out at 25°C in a Lunaire CE0932-2 environmental chamber (Williamsport, PE). The PDA and the RI detectors were placed in series, with measured dead volumes of 0.16 and 0.42 mL, respectively. The RI detector was mainly used. The PDA UV detector was used only for secondary detection, because the UV cutoff values for many solutes were too low.

Different sample sizes and dilution ratios (10 to 80 times) were tested in single component pulse tests, to ensure that the retention times observed were within the

linear isotherm range. The solvent itself was used as the diluent. The data reported here are for 20 μL injection pulses. The retention times were corrected for the dead-time (time spent in the extra-column dead volume).

In order to compare the relative strengths of solutes, the retention time t_{ref} of TTBB was used (see Section 3) as a reference to calculate the capacity factors k of all solutes, as

$$k \equiv (t - t_{ref})/t_{ref}$$

TTBB was also used as a "standard" at the beginning and at the end of each set of experiments, to test the apparatus stability. No significant changes in the retention time and plate number of TTBB were observed, indicating good reproducibility. The standard deviation in the capacity factors for TTBB in seven data sets was around 0.02 ($\Delta t = 0.1$ min). The flowrate Q was 1 mL/min. No significant variations in k were observed between $Q = 0.3$ and 3 mL/min.

3 Results and discussion

3.1 ATR-IR results of the effects of solutes on the ADMPC polymer structure

The IR spectrum of the polymer upon sorption of different solutes is also shown in Fig. 2. The IR spectrum of the dry ADMPC polymer is shown here for reference. Because the bands in the region from 3100 to 2800 cm^{-1} overlap with some solute peaks, they are not analyzed in detail. The main focus is bands in the region from 1800 to 1500 cm^{-1}: The amide I band, at 1750–1700 cm^{-1} is mainly due to C=O stretching, the amide II band, centered at 1541 cm^{-1}, is mainly due to NH bending, and the aromatic bands at 1616 cm^{-1} with a shoulder at 1604 cm^{-1} are also examined.

The amide I band of the dry polymer (Table 2 and Fig. 2) has two broad overlapping peaks, A and B, centered at 1745 cm^{-1} and 1717 cm^{-1}, respectively.

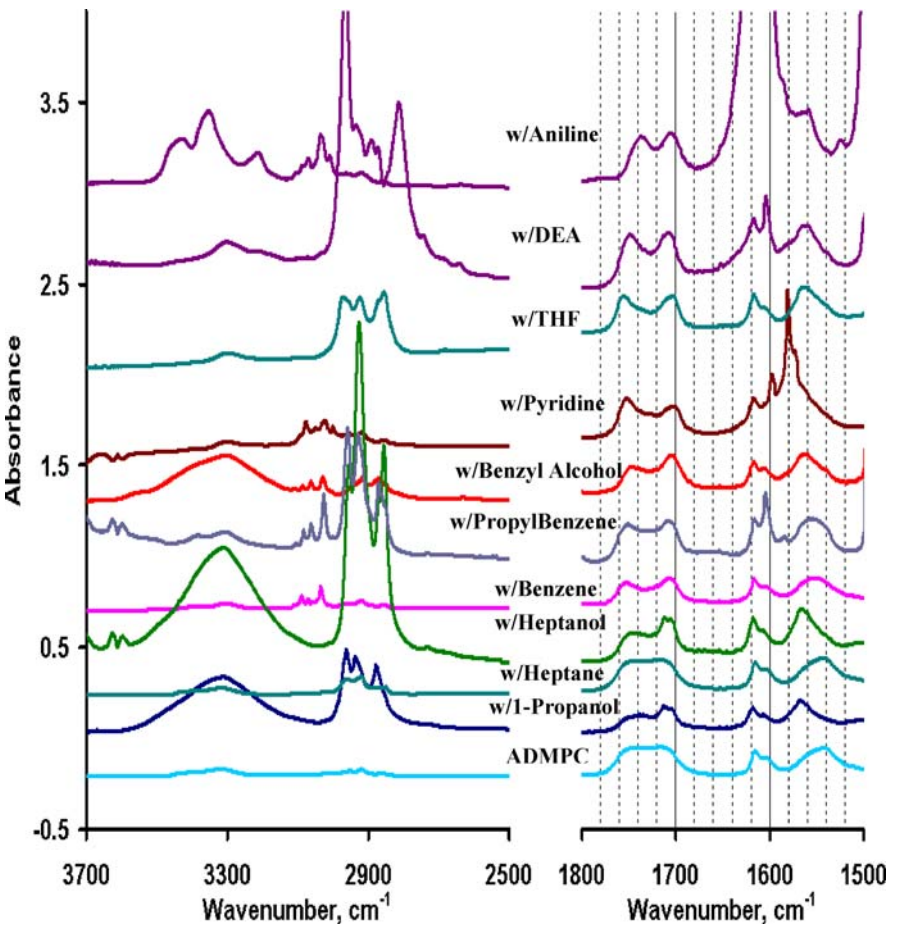

Fig. 2 IR spectra of ADMPC polymer in the dry state and upon equilibration with various solutes, as indicated. In the range 3700–2500 cm^{-1}, mostly the solute bands are observed. For improved clarity, the wavenumber scale in the range 1800–1500 cm^{-1} was enlarged about three-fold, and some gridlines are shown. Since no bands are observed in 2500–1800 cm^{-1} range, this range is not shown

Table 2 Measured IR wavenumbers for different amide and phenyl bands of dry ADMPC polymer and polymer in the presence of different solutes; see Fig. 2

	IR wavenumbers[a]			
	Amide I (cm^{-1})		Phenyl peaks (cm^{-1})	Amide II (cm^{-1})
System	A (weak H-bond)	B (strong H-bond)		
Dry Polymer	1745	1717	1615	1542[b]
Polymer with 1-Propanol	1734	1713	1618	1567
Polymer with Heptane	1746	1716	1615	1543
Polymer with Heptanol	1740	1712	1617	1566
Polymer with Benzene	1752	1707	1616	1550
Polymer with Propylbenzene	1751	1708	1616	1552
Polymer with Benzyl Alcohol	1747	1705	1617	1564
Polymer with Pyridine	1751	1701	1617	–
Polymer with THF	1755	1703	1617	1564
Polymer with DEA	1750	1707	1616	1559
Polymer with Aniline	1738	1706	1619	1558

[a]Amide I: 80% C═O stretching and 20% NH bending.
Amide II: 60% NH bending and 40% CN stretching.
[b]It has a shoulder at $\sim$1558 cm^{-1}.

The amide I wavenumber is known to decrease as the H-bond between the C═O and H─N groups becomes stronger (Pimentel and McClellan, 1960). Hence, band A is assigned mainly to C═O 'weakly H-bonded' to H─N, and band B is assigned mainly to C═O 'strongly H-bonded' to H─N. We recognize that each band includes a distribution of H-bonding strengths, which depend on the distances and orientations between the hydrogen donors and acceptors. We postulate that the weak H-bonds between the C═O and NH groups in the dry polymer are due mainly to groups from rods of different polymer chains (inter-rod, rather than intra-rod). By contrast to the amide I, the wavenumber of the amide II group (mainly NH bending) increases as the H-bond becomes stronger (Pimentel and McClellan, 1960). The amide II band (Fig. 2) lineshape can also be separated into two peaks, consistently with the amide I band, also indicating two populations, with distributed wavenumbers of mainly C═O$\cdots$H─N weak or strong H-bonds.

Here we report the IR spectra for ten solutes (some of them can also be used as solvents) listed in Table 1. With the absorption of 1-propanol by the polymer (Fig. 2 and Table 2), the ratio of the intensities of the two peaks A and B of the amide I changes. The intensity of the peak B increases, and the center of the band shifts to a lower wavenumber (from 1717 to 1713 cm^{-1}), indicating a relative increase in the population of strongly H-bonded C═O groups. The wavenumber of the center of the amide II band also changes significantly, from 1542 to 1567 cm^{-1}, indicating that the polymer NH groups make stronger H-bonds with 1-propanol molecules than those within the polymer. The presence of excess of 1-propanol in the sample is evident from the large H-bonded OH stretching and CH_3 bands. Moreover some small, $\sim$3 cm^{-1}, changes in the wavenumbers of the phenyl groups suggest some weak dipole-dipole interactions of the phenyl groups with 1-propanol. All the changes observed in the polymer spectrum are reversible after the complete removal of the 1-propanol by drying. From these results, we infer that 1-propanol interacts with the polymer, mainly via strong H-bonding interactions (Table 1) as follows: C═O (polymer)$\cdots$HO(1-propanol) and NH(polymer)$\cdots$OH(1-propanol). The changes in the H-bonded distribution of the C═O groups (amide I), and the changes in the wavenumbers of the amide II band, are due to the incorporation (absorption) of 1-propanol in the structure of the polymer. In the presence of 1-propanol, some percentage of the C═O$\cdots$HN H-bonds in and between the rods of the dry polymer are broken, and new stronger H-bonds are formed with the solute molecules, thereby changing the bulk structure of the polymer. Upon absorption of heptanol, the spectral changes observed are similar to those observed with 1-propanol.

The polymer spectrum remains essentially unchanged upon absorption of excess of non-polar heptane (Fig. 2 and Table 2). The wavenumbers of all the bands remain almost unchanged, within the experimental error, or reproducibility, of $\pm 1\,cm^{-1}$ (which is slightly less than the formal resolution of $\pm 2\,cm^{-1}$). The presence of excess heptane during the IR experiment is again established by the observed CH stretching bands in the 3000–2800 cm^{-1} region. We infer that heptane shows weak interactions, probably due to dispersion forces, but no strong H-bonding with the polymer, causing minimal changes in the intra-rod and inter-rod H-bond interactions and the overall polymer structure.

Upon absorption of benzene, the presence of excess benzene is evident from peaks in 3100 cm^{-1} region. The wavenumber of amide II band shifts from 1542 to 1550 cm^{-1}. Benzene acts as a weak acceptor compared to alcohols (Scheiner, 1997; Meyer et al., 2003), resulting in weaker H-bond interactions with the polymer NH groups. The fractional polarity of the benzene due to dipole interactions is relatively higher than that of an alcohol (Snyder et al., 1997). This results in strong dipole-dipole interactions of benzene with the polymer C=O groups. One can also expect weak H-bond interactions between benzene CH groups and the polymer C=O groups. Due to these dipole interactions, the wavenumber of band A now increases from 1745 to 1752 cm^{-1}, opposite to the effect of the alcohols. The peak B wavenumber shows downshift from 1717 to 1707 cm^{-1}. The possible, and often established (Meyer et al., 2003), π-π (aromatic-aromatic) interactions between the polymer phenyl groups and benzene are weak compared to H-bonding and can not be probed directly with IR. Results obtained for propylbenzene are similar to those for benzene. From these results, we infer that benzene and propylbenzene both interact with the polymer NH groups via weak H-bond interactions and with the polymer C=O groups via mainly dipole-dipole interactions.

With benzyl alcohol ($C_6H_5CH_2OH$) containing two potential functional groups, the broad OH stretching band of H-bonded benzyl alcohol is evident at 3300 cm^{-1} upon the absorption of benzyl alcohol by the polymer. The ratio of the intensities of the two peaks A and B of the amide I changes. The intensity of the peak B increases, and the center of the band B shifts to a lower wavenumber (from 1717 to 1705 cm^{-1}), indicating an increase in the strongly H-bonded C=O groups similarly to that of 1-propanol. The intensity of band A decreases, as with the alcohols. The wavenumber of band A shows an increase, rather than a decrease, compared to the dry polymer (Table 2), possibly due to dipole-dipole interactions of the phenyl groups with the polymer C=O groups, as with benzene. The wavenumber of the center of the amide II band also changes significantly from 1542 to 1564 cm^{-1}, indicating that the polymer NH groups make strong H-bonds with the OH groups of the benzyl alcohol molecules. From these results, we again infer that the OH groups of benzyl alcohol interact with the polymer, mainly via strong H-bonding interactions with the C=O and NH groups of the polymer, and the phenyl groups interact strongly with the polymer C=O groups via dipole-dipole interactions.

With absorption of pyridine (C_6H_5N) by the polymer (Fig. 2 and Table 2), a different trend compared to the results of alcohols, is observed in the intensities of the A and B bands of amide I. The intensity of band A increases compared to that of the band B. The increase in the band A may result from the breakup of a large portion of the C=O···HN H-bonds in and between the rods of the dry polymer because of the formation of strong NH(polymer)···N(pyridine) H-bond resulting in more "free" C=O groups. One can see changes in the amide II band (even though the pyridine peak overlaps) from strong NH···N H-bond interactions. The changes observed in the amide I band upon absorption of pyridine, can also be attributed to dipole-dipole interactions of the polymer C=O groups with pyridine, since the fractional polarity of which due to dipole interactions is significantly higher than that of alcohol (Snyder et al., 1997).

With absorption of THF (C_4H_8O) by the polymer (Fig. 2 and Table 2), certain bands of THF are observed in the, 3000–2800 cm^{-1} region. The observed change in the amide II band from 1542 to 1564 cm^{-1} is evidently due to strong H-bond between the oxygen atoms of THF and the NH groups of the polymer (Table 1). The intensity ratio of the two peaks A and B of the amide I changes. The wavenumber of band A increases significantly to 1755 cm^{-1}, possibly from the breakup of a large portion of the C=O···HN H-bonds in and between the rods of the dry polymer because of the formation of strong NH(polymer)···O(THF) H-bond, similarly to the pyridine results. The peak B wavenumber decreases significantly to 1703 cm^{-1}, because the wavenumber of the C=O group (amide I) is affected significantly by the strong NH(polymer)···O(THF)

Table 3 Calculated IR wavenumbers for amide I and amide II bands of ADMPC side-chain alone and in the presence of different solutes using the *DFT/B3LYP/6-311+g(d,p)* level of theory

System	Interaction	ΔE^a (kcal/mol)	H-Bond Distance (Å)	H-Bond Angle (°)	Wavenumbers (cm^{-1}) C=O (Amide I)	Wavenumbers (cm^{-1}) NH (Amide II)
Polymer side-chain only	–	–	–	–	1717	1512
With heptane	C=O···HC	(<0.5)	N/A	N/A	1716	1512
	NH···CH	(<0.5)	N/A	N/A	1718	1511
With 1-Propanol	C=O···HO	**−4.27**	1.97	168	1700	1515
	NH···OH	**−5.47**	2.00	158	1721	1549
With Benzene	C=O···HC	**−0.88**	2.50	179	1711	1513
With pyridine	NH···N	**−5.12**	2.05	177	1708	1546
With THF	C=O···HC	**−4.29**	2.50	168	1713	1513
	NH···O	**−7.95**	1.95	179	1710	1543
With DEA	NH···NH	**−4.93**	2.04	176	–	–

[a] Bold: BSSE corrected energy values.

H-bond (see Section 3.3). We also infer that the changes observed in the amide I band can also result from dipole-dipole interactions of the amide I group with THF (Snyder et al., 1997).

Upon absorption of DEA ($C_4H_{10}NH$), the wavenumbers of the amide bands I and II also change. The amide II band change is evidently caused by H-bonds of the NH groups of DEA with the NH groups of the polymer. The changes in the amide I band are caused in part by the dipole-dipole interactions of DEA. Because DEA is not acidic (Snyder et al., 1997), no H-bonds with the C=O groups are expected. The presence of excess DEA can be observed in the 3000–2800 cm^{-1} region.

The bands due to excess of aniline ($C_6H_5NH_2$) are observed in the 1570–1650 cm^{-1} region. Upon absorption of aniline, the wavenumbers of the polymer amide I and amide II bands change. The amide II band is now seen as a shoulder at 1558 cm^{-1} to the strong aniline band. The shift to 1558 cm^{-1} indicates H-bond interactions between NH groups of the polymer and NH_2 groups of aniline. Changes in the amide I wavenumbers are possibly due to dipole-dipole interactions of C=O with the phenyl ring and also due to H-bond interactions of C=O with the NH_2 groups.

3.2 DFT calculations of side-chain of the polymer with the solute molecules

DFT calculations for one side-chain of the polymer (Fig. 1) yielded the structure with minimum energy (Fig. 3). For this structure the predicted wavenumbers of the amide I and II bands are 1717 and 1512 cm^{-1}, respectively (Table 3). These simulations correspond to completely free amide I and II groups in the experiments, since no intra- or inter-rod H-bonds (which are inferred from the IR data) are considered in the simulations. By contrast, most of these bands in the experiments arise from intra-rod and inter-rod interactions (Fig. 2). The predicted values differ by 4% or less from the experimental values of 1790 and 1500 cm^{-1}. The accuracy is fair, considering that the calculations account only for one side-chain of the polymer.

DFT results for the complex formation between the polymer side-chain and some of the solutes are shown in Table 3. The energies of polymer-propanol range from 4 to 6 kcal/mol, indicating strong complex formations with strong H-bond interactions for both conformations (sketched in Fig. 3). The C=O···HO and NH···OH distances are quite short, and the angles, 168° and 158°, are significantly greater than 90°. Upon H-bond formation, the predicted amide I band wavenumber decreases, and that of the amide II increases, consistently with the IR data (Table 2). With heptane, the interaction energies are less than 0.5 kcal/mol (Table 3). No H-bonds are inferred from the calculated energies, distances, and angles. The predicted IR wavenumbers for the polymer-heptane remain essentially unchanged compared to those of the dry polymer, indicating again no H-bond formation, and they are consistent with the IR data. The predicted interactions between the polymer and the non-polar heptane have to be weak dispersion interactions.

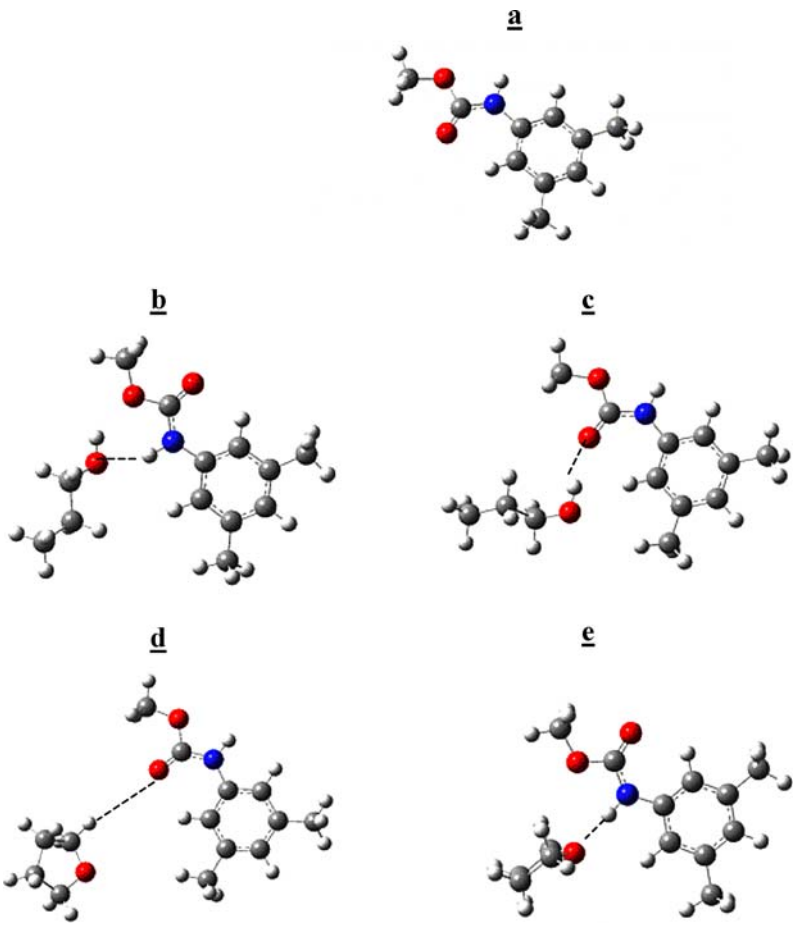

Fig. 3 Molecular structures, as predicted by Gaussian 03 of: (a) ADMPC polymer side-chain; (b) polymer side-chain complexed with 1-propanol in the following configuration, NH(polymer)· · ·OH(1-propanol); (c) polymer side-chain complexed with 1-propanol in a different configuration, C═O(polymer)· · ·HO(1-propanol); (d) polymer side-chain complexed with THF [C═O(polymer)· · ·HC(THF)]; (e) polymer side-chain complexed with THF [NH(polymer)· · ·O(THF)]. The dashed lines indicate the H-bonds

The energy of a certain polymer-benzene conformation is around 1 kcal/mol, indicating a weak H-bond interaction. The significant changes observed in amide I band IR data (Section 3.1) can not be explained by this weak H-bond. This inference supports our previous hypothesis that the changes observed in amide I band is mainly due to the dipole-dipole interaction between benzene and polymer C═O groups. With pyridine, in the NH(polymer)· · ·N(pyridine) configuration, the interaction energy is 5 kcal/mol indicating strong H-bond interaction. The H-bond distance is quite short, and the angle is significantly greater than 90°. The wavenmber of the amide II band increases, consistently with the IR data of Section 3.1. Surprisingly, the wavenumber of the amide I band decreases significantly in this configuration from 1717 to 1708 cm^{-1}, suggesting that the NH· · ·N H-bond also changes the electron distribution at C═O group and affects the wavenumber. The change observed in the band B wavenumber (Table 2) can be accounted by this simulation.

The energy of polymer-THF NH· · ·O conformation is 7.95 kcal/mol, indicating strong complex formation with strong H-bond interactions (Fig. 3(e)). The wavenumber of the amide II band increases consistently with IR data of Section 3.1. The wavenumber of the amide I band decreases, similarly to the pyridine result, again confirming that the strong NH· · ·O H-bond changes the electron distribution at the C═O group and affects the wavenumber. Surprisingly, the energy of the C═O(polymer)· · ·HC(THF) conformation (Fig. 3(d)) is 4.29 kcal/mol, which is more than one would expect assuming a weaker H-bond interaction between the polymer C═O groups and the THF CH groups. This may be due to possible dipole-dipole interactions between the polymer and THF. The energy of polymer-DEA NH· · ·NH conformation is 4.93 kcal/mol indicating strong H-bond interactions (Table 3).

3.3 Dependence of the capacity factors on the molecular structures of solutes

The chromatographic retention times, and the capacity factors of simple molecules generally depend on solute-sorbent, solvent-sorbent, and solute-solvent interactions. The solvent hexane/IPA used (95/5, v/v) in this study forms weak H-bonds with the sorbent and the solutes. The HPLC results with the simple non-chiral molecules indicate indirectly which functional groups of the solutes play important roles in the capacity factors. Combined with the more qualitative IR and quantitative DFT results, chromatographic capacity factors can be better elucidated.

The capacity factors provide some measures of the strengths of the relative interactions between the sorbent and solute functional groups. Since 1-propanol is both a strong H-bond donor and strong H-bond acceptor (Scheiner, 1997), it should form strong H-bonds with the sorbent (Sections 3.1 and 3.2), resulting in high capacity factors, $k = 1.4$ compared to $k = 0.02$ for heptane (Table 4). Being non-polar, heptane forms no H-bonds and shows weak interactions (see IR and DFT results), probably due to dispersion forces, resulting in a very low k-value. Moreover, the expected strong hydrophobic interactions of heptane with the hydrophobic solvent should produce a low capacity factor. For heptanol, the OH groups make H-bonds with the sorbent C=O and NH groups, resulting in the higher capacity factor of heptanol compared to heptane. Because of the moderate solute-solvent hydrophobic interactions for heptanol, its capacity factor is slightly lower than that of 1-propanol.

Table 4 Capacity factors of simple solutes on ADMPC[a]

#	Solute	Potential functional groups	k[b]
1	1-Propanol	OH, CH_3	1.39
2	Heptane	CH_3	0.02
3	1-Heptanol	OH, CH_3	1.00
4	Benzene	Ph	0.18
5	Propylbenzene	Ph, CH_3	0.10
6	Benzyl Alcohol	OH, Ph, CH_2	2.52
7	Pyridine	Ph, N	1.19
8	Tetrahydrofuran	CH_2, O	0.45
9	Diethylamine	NH, CH_3	0.64
10	Aniline	Ph, NH_2	2.52

[a]HPLC conditions: column size, 100 mm × 10 mm i. d.; flow rate, 1.0 ml/min; column temperature, 25°C; detector, RI; injection volume, 20 μL; solvent, hex/IPA (95/5, v/v).
[b]All capacity factors are calculated using the retention time of TTBB ($t_{ref} = 4.96$ min) as a reference.

For benzene the k-value is higher than for heptane, 0.18 vs. 0.02 probably because of the interactions of benzene with the sorbent phenyl groups. The dipole-dipole interactions of benzene with polymer C=O groups can also contribute to the k value. Even though benzene usually acts as a weak H-bond acceptor (Levitt and Perutz, 1988), and hence it can interact with the sorbent NH groups via weak H-bond interactions as observed in IR, the aromatic-aromatic (π-π) interactions should be significant, as reported by Meyer et al. (2003). The addition of a propyl group to benzene (in propylbenzene) causes a slight decrease in the capacity factor, 0.18 vs. 0.10, apparently because of the expected stronger solute-solvent hydrophobic interactions. Exchanging an H atom in benzene with a CH_2OH group, as in the benzyl alcohol, increases the capacity factor to 2.52. We infer strong solute-sorbent H-bond interactions for benzyl alcohol. Exchanging H in benzene by an NH_2 group, as in aniline, again increases the capacity factor to 2.52, because of strong solute-sorbent H-bond interactions.

The introduction of an heteroatom into the aromatic ring has a significant influence on the aromatic-aromatic interactions (Meyer et al., 2003). k of pyridine was measured and it was found to be $k = 1.9$, significantly higher than for benzene. Pyridine is expected to interact via H-bonds of the lone electron pair on the nitrogen with the sorbent NH groups as shown in DFT results (Table 3) and via aromatic-aromatic interactions. Moreover, pyridine may interact with the sorbent C=O groups via dipole-dipole interactions. These effects can account for the high pyridine capacity factor.

For THF it was found that $k = 0.45$. Apparently, the combined effects of the dipole-dipole interactions and the H-bond interactions of the O atom in THF with the NH group of the sorbent may have caused a higher capacity factor for THF than for benzene, consistent with the DFT results. The capacity factor for DEA is higher compared to heptane (0.64 vs. 0.15), evidently because of the strong solute-sorbent H-bond interactions (Table 3) and also dipole-dipole interactions. Hence, the combination of IR, DFT, and chromatography results, with a systematic variation of the solute molecular structure, allows for plausible rational molecular interpretation of the observed retention times or capacity factors.

4 Conclusions

In the present study, a series of simple non-chiral solutes, 1-propanol, heptane, heptanol, benzene, propylbenzene, benzyl alcohol, pyridine, tetrahydrofuran, diethylamine, and aniline, is used to elucidate the solvent-sorbent, solute-sorbent, and solute-solvent interactions with Chiralpak AD sorbent in hexane/IPA (95/5, v/v) solvent. H-bonding, hydrophobic, or dipole-dipole are the main types of such interactions. The H-bonding and dipole-dipole interactions of ADMPC polymer C═O and NH groups with the functional groups of these solutes, primarily OH, NH, NH_2, O, phenyl, and N, are studied, mostly qualitatively by IR, and mostly quantitatively by DFT modeling. DFT modeling of the polymer side-chains interacting with some of these solutes at various configurations provide energies of H-bonding or other interactions and predictions of the IR wavenumbers of the amide I and amide II bands. The predicted trends in the shifts of the wavenumbers due to the H-bonding agree with the data. Using the IR data and DFT modeling, we have established that the C═O and NH groups of ADMPC are the key binding sites of this polymer. The chromatographic capacity factors of the solutes at 25°C with 95/5 (v/v) hexane-isopropanol solvent are linked to the details of their molecular structures, namely the types of the functional groups. They can be understood from hydrogen bonding and dipole-dipole polymer-solute interactions. These results have implications in understanding more complex sorbent-solute interactions of other complex chiral molecules.

Nomenclature

t_{ref}	Retention time for reference solute (TTBB) in min.
t	Retention time for a solute in min.
k	Capacity factor for a solute; $\equiv (t - t_{\text{ref}})/t_{\text{ref}}$.
Δt	Standard deviation in the capacity factors for TTBB in seven data set.
Q	Flow rate, mL/min
ε_p	Intraparticle void fraction
ε_b	Interparticle void fraction

Acknowledgments We thank Dr. Geoff Cox, Chiral Technologies, for providing the chiral columns used in this study, and for helpful discussions. We thank Ms. Debby Sielegar and Ms. Siao Yee Wee for their help in some of the experiments. This research was supported in part by the National Science Foundation (NSF) grant CTS-0625189.

References

Agranat, I. et al., "Putting Chirality to Work: The Strategy of Chiral Switches," *Nature Review Drug Discovery*, **1**(10), 753–768 (2002).

Andersson, M.P. and P. Uvdal, "New Scale Factors for Harmonic Vibrational Frequencies Using the B3LYP Density Functional Method with the Triple-ú Basis Set 6–311+G(d,p)," *J. Phys. Chem. A*, **109**, 2937 (2005).

Armstrong, D.W. and W. Demond, "Cyclodextrin Bonded Phases for the Liquid-Chromatographic Separation of Optical, Geometrical, and Structural Isomers," *J. Chromatogr. Sci.*, **22**(9), 411–415 (1984).

Armstrong, D.W. et al., "Macrocyclic Antibiotics as a New Class of Chiral Selectors for Liquid-Chromatography," *Anal. Chem.*, **66**(9), 1473–1484 (1994).

Becke, A.D., J. "Density-Functional Thermochemistry. 3. The Role of Exact Exchange," *Chem. Phys.*, **98**, 5648 (1993).

Booth, T.D. and I.W. Wainer, "Investigation of the Enantioselective Separations of Alpha-Alkylarylcarboxylic Acids on an Amylose tris(3,5-dimethylphenylcarbamate) Chiral Stationary Phase Using Quantitative Structure-Enantioselective Retention Relationships—Identification of a Conformationally Driven Chiral Recognition Mechanism," *J. Chromatogr. A*, **737**(2), 157–169 (1996).

Caccamese, S. and G. Principato, "Separation of the Four Pairs of Enantiomers of Vincamine Alkaloids by Enantioselective High-Performance Liquid Chromatography," *J. Chromatogr. A*, **893**(1), 47–54 (2000).

Chilmonczyk, Z. et al., "Enantioselective Separation of 1,4-disubstituted Piperazine Derivatives on Two Cellulose Chiralcel OD and OJ and one Amylose Chiralpak AD Chiral Selectors," *Chirality*, **11**(10), 790–794 (1999).

Frisch, M.J.T., Gaussian 03. Wallingford CT (2004).

Goossens, J.F. et al., "Column Selection and Method Development for the Separation of Nucleoside Phosphotriester Diastereoisomers, New Potential Anti-Viral Drugs. Application to Cellular Extract Analysis," *Biomed. Chromatogr.*, **19**(6), 415–425 (2005).

Jadaud, P. and I.W. Wainer, "Stereochemical Recognition of Enantiomeric and Diastereomeric Dipeptides by High-Performance Liquid-Chromatography on a Chiral Stationary Phase Based Upon Immobilized Alpha-Chymotrypsin," *J. Chromatogr.*, **476**, 165–174 (1989).

Lammerhofer, M. and W. Lindner, "Quinine and Quinidine Derivatives as Chiral Selectors.1. Brush Type Chiral Stationary Phases for High-Performance Liquid Chromatography Based on Cinchonan Carbamates and their Application as Chiral Anion Exchangers," *J. Chromatogr. A*, **741**(1), 33–48 (1996).

Lee K.B. et al., "Standing-Wave Design of a Simulated Moving Bed Under a Pressure Limit for Enantioseparation of Phenylpropanolamine," *I & ERC*, **44**(9), 3249–3267 (2005).

Levitt, M. and M.F. Perutz, "Aromatic Rings Act as Hydrogen-Bond Acceptors," *J. Mol. Biol.*, **201**(4), (1988).

Meyer, E.A., et al., "Interactions with Aroamatic Rings in Chemical and Biological Recognition," *Angew. Chem. Int. Ed.*, **42**(11), 1210–1250 (2003).

Meyer, M. et al., "Density Functional Study of Guanine and Uracil Quartets and of Guanine Quartet/Metal Ion Complexes," *J. Comp. Chem.*, **22**(1), 109 (2001).

Okamoto, Y. et al., "Chromatographic Resolution.17. Useful Chiral Stationary Phases for Hplc–Amylose Tris(3,5-Dimethylphenylcarbamate) and Tris(3,5-Dichlorophenylcarbamate) Supported on Silica-Gel," *Chem. Lett.*, (9), 1857–1860 (1987a).

Okamoto, Y. et al., "Chromatographic Chiral Resolution.14. Cellulose Tribenzoate Derivatives as Chiral Stationary Phases for High-Performance Liquid-Chromatography," *J. Chromatogr.*, **389**(1), 95–102 (1987b).

Okamoto, Y. and E. Yashima, "Polysaccharide Derivatives for Chromatographic Separation of Enantiomers," *Angew. Chem. Int. Ed. Engl.*, **37**, 1020–1043 (1998).

Pimentel, G.C. and A.L. McClellan, *The Hydrogen Bond*, San Francisco, W.H. Freeman, 1960.

Pirkle, W.H. et al., "Broad-Spectrum Resolution of Optical Isomers Using Chiral High-Performance Liquid-Chromatographic Bonded Phases," *J. Chromatogr.*, **192**(1), 143–158 (1980).

Scheiner, S. *Hydrogen Bonding: A Theoretical Perspective*, New York, Oxford University Press, 1997.

Simon, S. et al., "How does Basis Set Superposition Error Change the Potential Surfaces for Hydrogen Bonded Dimers?," *J. Chem. Phys.*, **105**(24), 11024–11031 (1996).

Snyder, L.R. et al., *Practical HPLC Method Development,* Wiley-Interscience, 1997.

Wang, T. et al., "Enantiomeric Separation of Some Pharmaceutical Intermediates and Reversal of Elution Orders by High-Performance Liquid Chromatography Using Cellulose and Amylose tris(3,5-dimethylphenylcarbamate) Derivatives as Stationary Phases," *J. Chromatogr. A*, **902**(2), 345–355 (2000).

Wenslow, R. and T. Wang, "Solid-State NMR Characterization of Amylose Tris (3,5-dimethylphenylcarbamate) Chiral Stationary-Phase Structure as a Function of Mobile-Phase Composition," *Anal. Chem.*, **73**, 4190–4195 (2001).

Yamamoto, C. et al., "Structural Analysis of Amylose Tris(3,5-dimethylphenylcarbamate) by NMR Relevant to its Chiral Recognition Mechanism in HPLC," *J. Am. Chem. Soc.*, **124**(42), 12583–12589 (2002).

Yashima, E., "Polysaccharide-Based Chiral Stationary Phases for High-Performance Liquid Chromatographic Enantioseparation," *J. Chromatogr. A*, **906**(1–2), 105–125 (2001).

Yashima, E. and Y. Okamoto, "Optically Active Polymers for Chiral Separations," *Bull. Chem. Soc. Jpn.*, **77**(2), 227–257 (2004).